CCIT Report #613
February 2007

Illumination Multiplexing within Fundamental Limits

Netanel Ratner Yoav Y. Schechner
Dept. Electrical Engineering
Technion - Israel Inst. Technology
Haifa 32000, ISRAEL
ratner@tx.technion.ac.il yoav@ee.technion.ac.il

Abstract

Taking a sequence of photographs using multiple illumination sources or settings is central to many computer vision and graphics problems. Recently, a growing number of methods use multiple sources rather than single point sources in each frame of the sequence. Potential benefits include increased signal-to-noise ratio and accommodation of scene dynamic range. However, existing multiplexing schemes, including Hadamard-based codes, are inhibited by fundamental limits set by Poisson distributed photon noise and by sensor saturation. The prior schemes may actually be counterproductive due to these effects. We derive multiplexing codes that are optimal *under these fundamental effects. Thus, the novel codes* generalize *the prior schemes and have a much broader applicability. Our approach is based on formulating the problem as a constrained optimization. We further suggest an algorithm to solve this optimization problem. The superiority and effectiveness of the method is demonstrated in experiments involving object illumination.*

1. Illumination Multiplexing

In computer vision research and image-based rendering, objects or people are often acquired under variable lighting directions [3, 5, 7, 16, 17, 20, 21, 22, 23, 28, 29, 31, 34, 35, 40]. Such images are then used for object recognition and identification [3, 16, 25, 27, 34, 35], rendering [6, 16, 23, 29], shape estimation [10, 12, 13, 14, 39, 40] and analysis of specularities, shadows and occlusions [30]. Traditionally, such images were taken by moving a light source around the object, or by sequential operation of individual sources in a constellation. However, recently, there is growing interest in using illumination which is not based on single point sources. Rather, it is based a sequence of images, in each of which lighting may simultaneously arrive from several directions or sources [5, 16, 18, 24, 31, 32, 33, 37]. Some of the benefits include significant improvement in signal noise ratio (SNR) [32] (See for example Fig. 1), significant reduction of dynamic range problems in the presence of saturated pixels, and convenience when photographing people [37]. Other advantages mentioned are efficiency of the acquisition process and image representation, and image enhancement by simultaneous use of flashes and ambient lighting.

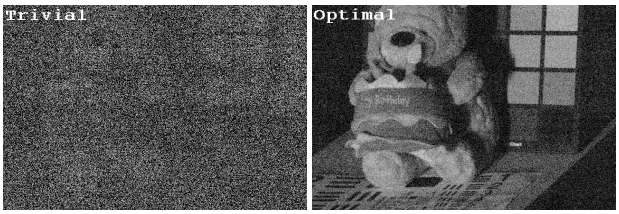

Figure 1. [Left] An image taken under a single light source. [Right] An image of the same scene, decoded from multiplexed illuminated objects. It is decoded as if illuminated by the same single source. The multiplexing code is optimal.

The question is, given all the possibilities of simultaneous operation of sources, what is the optimal way to multiplex the sources in each frame. Ref. [32] suggested that Hadamard-based codes should be used. However, its analysis did not account for a very important problem: image noise depends on the image irradiance itself, which may make Hadamard multiplexing counter productive, as was later experienced by [37]. Fundamentally, this is due to *photon noise*, which exists even in images no matter the quality of the camera, as it stems from the quantum mechanical nature of light. Moreover, no prior study accounted for saturation when seeking optimal lighting. This is despite the acknowledgment that saturation and scene dynamic range are important aspects when using multiple sources [32, 37].

This paper directly seeks multiplexing codes that are optimal under the fundamental limitations of photon noise and saturation, in addition to camera readout noise. This problem and its solution have implications much broader than computer vision and graphics. The reason is that multi-

plexing of radiation sources is used in many sensing modalities, such as X-ray imaging [11, 36], spectroscopy [11], and communication in fiber optics. Hence, the approach we present here has wide applicability. It is based on a constrained optimization formulation. We also describe an algorithm for solving this problem. The novel codes resulting from it are superior to any prior multiplexing codes. We demonstrate this in experiments of object illumination.

2. Theoretical Background

2.1. Multiplexing

Consider a setup where N light sources illuminate an object from various directions. Let $\mathbf{i} = (i_1, i_2, \ldots, i_N)^t$ be a set of intensity values of a certain pixel, where each value corresponds to illumination by any *individual* light source in this setup. Here, t denotes transposition.

In general, several light sources can be turned on at a time (multiplexing). Define an $N \times N$ multiplex matrix $\mathbf{W}$. It is often referred to as "multiplexing code" Each element of its mth row represents the power of the corresponding illumination source in the mth measurement. The power is measured relative to its maximum value where, 0 states that the source is completely off and 1 indicates a fully activated source. The measurements acquired at each pixel are denoted by the vector $\mathbf{a} = (a_1, a_2, \ldots, a_N)^t$.It is given by

$$\mathbf{a} = \mathbf{W}\mathbf{i} + \upsilon \quad , \tag{1}$$

where υ is the measurement noise. Any bias to this noise is assumed to be compensated for. The noise υ, in different pixels is assumed to be uncorrelated, with variance of σ_a^2.

Once images have been acquired under multiplexed illumination, they can be demultiplexed computationally, to derive estimates for the pixel values under single-source illumination $\hat{\mathbf{i}}$. The best linear estimator in the sense of mean square error (MSE) for the single source images is

$$\hat{\mathbf{i}} = \mathbf{W}^{-1}\mathbf{a} \quad . \tag{2}$$

The MSE of this estimator [11, 32] is

$$\mathrm{MSE}_{\hat{\mathbf{i}}} = \frac{\sigma_a^2}{N}\mathrm{trace}\left[\left(\mathbf{W}^t\mathbf{W}\right)^{-1}\right] \quad . \tag{3}$$

This is the expected noise variance of the recovered images. The lower it is, the better the SNR. The ratio of the SNRs with and without multiplexing

$$G = \mathrm{SNR}_{\mathrm{Multiplexed}}/\mathrm{SNR}_{\mathrm{Single}} \tag{4}$$

is the *multiplex gain* We now discuss the noise mechanisms.

2.2. Noise Mechanisms

To analyze the effect of multiplexing, we should first understand the sources of image noise. In this section we briefly review the affine noise model, of high grade detectors, which have a linear radiometric response. The noise can be divided into two components, signal-dependent and signal-independent. Regardless of the photon flux, signal-independent noise is created by dark current [8, 15, 19], by amplifier noise and the quantizer in the camera circuity [19]. Denote the graylevel variance of signal-independent noise by κ_{gray}^2.

Signal-dependent noise is related to two random effects. The random nature of light's photon flux and the uncertainty in the process of electron-photon conversion in the detector. Overall, the random number $n_{\mathrm{electr}}^{\mathrm{photo}}$ of photo-generated electrons is Poisson distributed [1, 2, 8, 15]. In this distribution, the variance of $n_{\mathrm{electr}}^{\mathrm{photo}}$ is

$$\mathrm{VAR}(n_{\mathrm{electr}}^{\mathrm{photo}}) = \mathcal{E}(n_{\mathrm{electr}}^{\mathrm{photo}}) \quad . \tag{5}$$

This variance increases with the measured electric signal $n_{\mathrm{electr}}^{\mathrm{photo}}$. The number of detected electrons $n_{\mathrm{electr}}^{\mathrm{photo}}$ is proportional to the gray-level of the acquired pixel value a

$$a = n_{\mathrm{electr}}^{\mathrm{photo}}/Q_{\mathrm{electr}} \quad . \tag{6}$$

Here Q_{electr} is the number of photo-generated electrons required to change a unit gray-level. Typically $Q_{\mathrm{electr}} \gg 1$. Combining Eqs. (5,6) yields the variance in gray levels

$$\mathcal{E}(n_{\mathrm{electr}}^{\mathrm{photo}})/Q_{\mathrm{electr}}^2 = a/Q_{\mathrm{electr}} \quad . \tag{7}$$

Compounded with signal-independent noise, the total noise variance of the measured gray level [8, 15] is

$$\sigma_a^2 = \kappa_{\mathrm{gray}}^2 + a/Q_{\mathrm{electr}} \quad . \tag{8}$$

Now, consider a diffuse object and sources that illuminate the object from similar directions. In this case, each light source yields a similar object radiance, hence, a similar photon noise. We rephrase Eq. (8) for the general case of C light sources activated in maximal intensity per measurement. Then,

$$\sigma_a^2 = \kappa_{\mathrm{gray}}^2 + C\eta^2 \quad \forall k \in \{1, \ldots, N\} \quad . \tag{9}$$

Here η^2 is the photon noise variance, induced by illuminating the object by a *single* source. This is an affine function of the number of sources C. Next, we describe the effect of the affine noise model on multiplexing.

As an example consider Fig. 2. It plots the average noise in raw images acquired by a PtGrey Dragonfly camera, as function of the number of sources being used. Fitting a straight line to this plot yields κ_{gray}^2 and η^2.

2.3. Photon Noise and Multiplexing

A well known multiplexing code is based on Hadamard codes. Its multiplex matrix known as the **S**-matrix [9, 11, 26, 32, 36, 37]. It was used in Refs. [32, 37] to multiplex illumination sources. In each row of the **S**-matrix, $(N+1)/2$

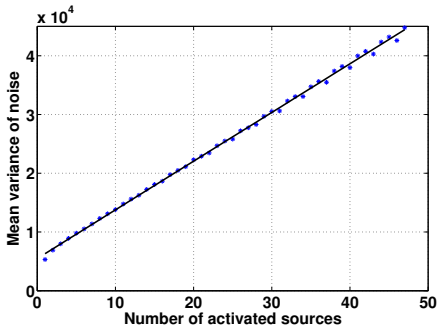

Figure 2. Results of the calibration process for 47 light sources. We see the noise variance, linearly increases with the number of used sources, in consensus with the affine noise model.

of the elements have the value of 1, while the rest are null. The MSE obtained using that code is

$$\mathrm{MSE}_{\hat{i},\mathrm{Had}} = \frac{4N}{(N+1)^2}\sigma_a^2 \quad . \tag{10}$$

Applying the affine noise model, (9) with $C = (N+1)/2$ in Eq. (10) yields

$$\mathrm{MSE}_{\hat{\mathbf{i}},\mathrm{Had}} = \frac{4N}{(N+1)^2}\kappa_{\mathrm{gray}}^2 + \frac{2N}{N+1}\eta^2 \quad . \tag{11}$$

In the special case where the photon noise is negligible, *i.e.* $\kappa_{\mathrm{gray}}^2 \gg C\eta^2$, Eq. (10) becomes:

$$\mathrm{MSE}_{\hat{\mathbf{i}},\mathrm{Had}} = \frac{4N}{(N+1)^2}\kappa_{\mathrm{gray}}^2 \tag{12}$$

and the corresponding SNR gain is [32, 38]

$$G_{\mathrm{Had}} = \frac{\mathrm{SNR}_{\mathrm{Hadamard}}}{\mathrm{SNR}_{\mathrm{Single}}} = \frac{N+1}{2\sqrt{N}} \quad . \tag{13}$$

Hence, in such a scenario, Hadamard multiplexing is highly beneficial. Ref. [11] shows that then, the **S**-matrix is optimal, minimizing Eq. (3).

On the other hand, when photon statistics dominate the noise, $C\eta^2 \gg \kappa_{\mathrm{gray}}^2$, Eq. (11) indicates that the demultiplexed images are *more* noisy than those obtained by simple single-source acquisition [11, 37]. The noise variance doubles by this process, if $N \gg 1$. The reason is that increasing the signal by multiplexing light sources, also increases the photon noise.

Ref. [38] looked into the problem of multiplexing under photon noise. It formulated a general expression for the multiplex gain under the affine model of Eq. (8):

$$G = G_0 \left(\frac{1+\chi^2}{1+C\chi^2}\right)^{\frac{1}{2}} \quad , \tag{14}$$

where $\chi = \eta/\kappa_{\mathrm{gray}}$. Here,

$$G_0 = \sqrt{N/\mathrm{trace}\left[\left(\mathbf{W}^t\mathbf{W}\right)^{-1}\right]} \tag{15}$$

is the multiplex gain when photon noise is not considered. Hence, for given parameters of the noise, G is maximized by reducing C while increasing G_0. Ref. [38] also found multiplexing codes based on *perfect sequences* for which G is optimal. However, the codes of Ref. [38] can only be applied to a very limited set of N and noise parameters. For most parameters and N values, the codes in [38] do not exist. Moreover, these codes apply only to cyclic matrices $\mathbf{W}$, hence they are not general.

3. Optimal Saturated Multiplexing

We begin the discussion about multiplexing codes under fundamental limits by considering saturation. While an object may be moderately bright when illuminated by a single source, it can become saturated if illuminated by numerous light sources. When this is the case, multiplexing too many sources, *e.g.* using the **S**-matrix is impractical. While exposure time may be reduced to counter saturation, Ref. [32] proved that such a step should be avoided: a better solution is to decrease the number of illumination sources C used in each measurement. This raises the need for new multiplexing codes, that comply with constraints on the number of light sources C used in each measurement.

Assume that the saturation phenomenon is insensitive to the specific identities of the illuminating sources. Saturation is assumed to occur when the total illumination radiance exceeds a threshold, C_{sat}. If all light sources have a similar radiance, then C_{sat} expresses units of light sources, and is analogous to C in Sec. 2.3.

Saturation is avoided if

$$\sum_{s=1}^{N} w_{m,s} \leqslant C_{\mathrm{sat}} \qquad \forall m \in \{1,2,\ldots,N\} \quad . \tag{16}$$

Recall that all sources can be activated with some portion of their maximum intensity *i.e.*

$$0 \leqslant w_{m,s} \leqslant 1 \qquad \forall m,s \in \{1,2,\ldots,N\} \quad . \tag{17}$$

We use Eq. (15) to formulate a maximization problem on the multiplex gain, G_0. This is equivalent to minimizing its reciprocal square *i.e.*

$$\arg\max_{\mathbf{W}} G_0 \equiv \arg\min_{\mathbf{W}} \frac{1}{G_0^2} = \arg\min_{\mathbf{W}} \frac{1}{N}\mathrm{trace}\left[\left(\mathbf{W}^t\mathbf{W}\right)^{-1}\right] \quad . \tag{18}$$

The constraints for our problem are taken from Eqs. (16,17). Thus, the optimization problem is

$$\min_{\mathbf{W}} \frac{1}{N}\mathrm{trace}\left[\left(\mathbf{W}^t\mathbf{W}\right)^{-1}\right] \tag{19}$$

$$\text{s.t.} \quad \mathbf{1}_{1,N}\cdot\mathbf{w}_m - C_{\mathrm{sat}} \leqslant 0 \qquad \forall m \in \{1,\ldots,N\} \tag{20}$$

$$-w_{m,s} \leqslant 0 \quad \forall m,s \in \{1,\ldots,N\} \tag{21}$$

$$w_{m,s} - 1 \leqslant 0 \quad \forall m,s \in \{1,\ldots,N\} \quad . \tag{22}$$

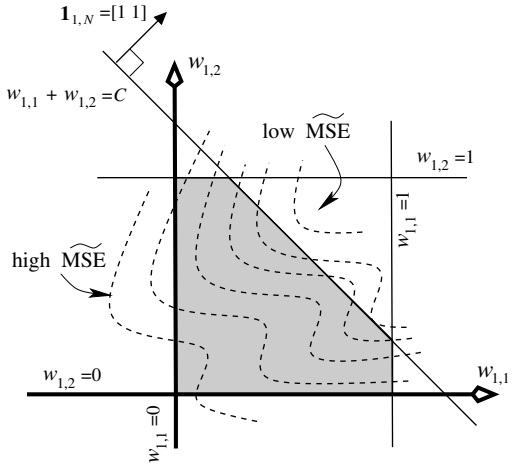

Figure 3. A 2D illustration of the optimization task. The shaded area is the domain in which $\mathbf{w}_1$ satisfies the constrains.

Here $\mathbf{1}_{1,N}$ is a row vector, all of whose elements are 1 and $\mathbf{w}_m$ is the m'th row of $\mathbf{W}$. See Fig. 3 for an illustration of this optimization task.

This problem is simple if $C_{\text{sat}} > (N+1)/2$. In this case, codes based on $\mathbf{S}$-matrix are optimal. The reason is that saturation is not met in Hadamard multiplexing when $C_{\text{sat}} > (N+1)/2$. Moreover, signal-dependent noise is not explicitly used in (19). Hence, the optimality [11] of Hadamard codes holds in this case.

We thus focus on $C_{\text{sat}} \leq (N+1)/2$. Simulations we preformed found local minima in (19). The best minimum occurred when (20) was active. This may be intuitively explained by arguing that one prefers to exploit maximum radiance for every measurement.[1] We therefore replace Eq. (20) by an equality constraint on the sum of rows *i.e.*

$$\mathbf{1}_{1,N} \cdot \mathbf{w}_m = C \qquad \forall m \in \{1, 2, \ldots, N\} \quad , \tag{23}$$

setting $C = C_{\text{sat}}$ in Eq. (23) facilitates optimization under saturation. Nevertheless, we maintain the use of C rather than C_{sat} to allow a later generalization to photon noise. Note that Eq. (23) means that $\mathbf{w}_m$ must lie on a hyperplane (see Fig. 3), whose unit normal vector is $(1/\sqrt{N})\mathbf{1}_{1,N}^t$.

4. Optimal Photon Limited Lighting

Sec. 3 considered only saturation. We now extend the approach presented in Sec. 3 to cope with photon noise. Solving the optimization problem in Eq. (19) subject to the constraints (21,22,23) results in an illumination matrix $\mathbf{W}(C)$, that is optimal, for a given C. In other words, we determine the values in each row $\mathbf{w}_m$ of $\mathbf{W}(C)$, such $\mathbf{1}_{1,N} \cdot \mathbf{w}_m$ is exactly C, while $\mathbf{W}(C)$ has the highest multiplex gain, G_0.

[1] This intuition holds if the noise is signal independent. The more general case is discussed in Sec. 4.

Eq. (14) converts G_0 to the gain under the general affine noise model.

We wish to note that there is no point in checking cases where $C \geqslant \frac{N+1}{2}$. They are certainly suboptimal, for a given N, as we no explain. Recall that for signal-independent noise and no saturation, G is optimized by the $\mathbf{S}$-matrix. From (14) it can also be seen that if G_0 is optimized, there is no point in increasing C, as it will only degrade G.

Recall that χ^2 can be obtained from calibration, as described in Sec. 2.2. Based of χ^2 and $G_0(\mathbf{W}(C))$, Eq. (14) yields the expected multiplexing gain $G(C)$. We now scan a range of values for C. For each C, we get $\mathbf{W}(C)$, as well as $G(C)$. Out of these, we select the value of C maximizing G. This scan finds the *number of illumination sources* that maximizes the gain. To recap,

1. Calibrate the system to find χ^2.
2. Scan the range of C values from 1 to C_{sat}. For each[2] value of C do the following:
3. Find the matrix $\mathbf{W}(C)$ that optimizes Eq. (19) subject to Eqs. (21,22,23).
4. Calculate the expected multiplex gain $G(C)$ using Eq. (14, 15).
5. Let $C_{\text{opt}} = \arg\max_C G(C)$.
6. The desired multiplex code is $\mathbf{W}(C_{\text{opt}})$.

5. Minimization Procedure

We now describe a numerical scheme for solving of the system given in Eqs. (19,21,22, 23). It consists of a *core*, which is based on a projected gradient method [4]. It also consists of a higher-level procedure, designed to escape local minima.

Define:

$$\widetilde{\text{MSE}} = \frac{1}{\sigma_a^2}\text{MSE}_{\hat{\mathbf{i}}}(\mathbf{W}) = \frac{1}{N}\text{trace}\left[\left(\mathbf{W}^t\mathbf{W}\right)^{-1}\right] \quad . \tag{24}$$

We iteratively minimize $\widetilde{\text{MSE}}$ as a function of $\mathbf{W}$. The minimization core is based on projected gradient descend. In each basic step, $\mathbf{W}$ is updated by the gradient

$$\mathbf{\Gamma} \triangleq \frac{d\widetilde{\text{MSE}}}{d\mathbf{W}} = -\frac{2}{N}\left(\mathbf{W}^t\mathbf{W}\mathbf{W}^t\right)^{-1} \quad . \tag{25}$$

The updated $\mathbf{W}$ is then projected onto constraints (17) and (23), one at a time. This is illustrated in Fig. 4. Further details are given in App. A.

The $\widetilde{\text{MSE}}$ in Eq. (19) is a multimodal function of $\mathbf{W}$. Therefore, the core generally converges to a local minimum, rather than a global one. To escape local minima, we embed the above core into a higher level process. When the core

[2] There is no necessity for exhaustive search of $G(C)$. As $G(C)$ is well behaved, one can incorporate efficient optimization procedures.

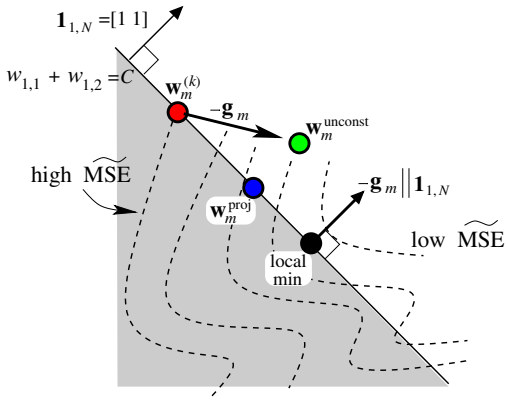

Figure 4. From $\mathbf{w}_m$ (red dot), gradient descend yields $\mathbf{w}_m^{\text{unconst}}$ (green dot). This is projected into the constraint (23), yielding $\mathbf{w}_m^{\text{proj}}$ (blue). When the gradient $\mathbf{g}_m$ is normal to the constraint surface, then $\mathbf{w}_m^{\text{proj}} = \mathbf{w}_m$ (black dot). Hence, the optimization gets stuck at a local minimum.

converges to a local minimum, $\mathbf{W}$ is modified, as we describe below. Then, the core is re-initialized with the modified $\mathbf{W}$.

The minimization core gets stuck in a local minimum because specific rows of $\mathbf{W}$ that are prevented from undergoing any modification. This prevention is caused by the *constraints*. To understand this, note that Eq. (25) is never nulled.[3] Hence, following the Karush-Kuhn-Tucker theorem [4], all of the extrema of $\widetilde{\text{MSE}}$ are obtained when at least some *constraints are active*. For this reason, local minima are caused by matrix rows which reside on constraints, as illustrated in Fig. 4. On the other hand, other rows of $\mathbf{W}$ are free to change. We therefore seek to identify rows that stagnate the minimization core.

The m'th row of $\mathbf{W}$ is $\mathbf{w}_m$. Its corresponding row in the gradient matrix $\mathbf{\Gamma}$ is $\mathbf{g}_m$. When $\mathbf{g}_m$ is parallel to $\mathbf{1}_{1,N}$, it means that this row of the gradient, is orthogonal to the constraint surface given in (23), as illustrated in Fig. 4. If this is the case, then $\mathbf{w}_m$ is equivalent to its projection, stagnating the minimization core. Hence, a sufficient condition of row m of $\mathbf{W}$ to stagnate is that $\mathbf{g}_m \parallel \mathbf{1}_{1,N}$.

While this condition is sufficient, it is not a necessary one. We now describe a wider class of stagnating rows. Suppose that $\mathbf{w}_m$ has elements s for which $w_{m,s} = 1$ or 0 and that $\mathbf{w}_m - \mathbf{g}_m$ shifts them beyond the bounds of Eqs. (21,22). Denote the set of indices of these elements by S^{overflow}. Now, define a row vector $\mathbf{g}_m^{\text{eff}} \in \mathbb{R}^{N-|S^{\text{overflow}}|}$. It is extracted from $\mathbf{g}_m$. It defined as $\mathbf{g}_m^{\text{eff}} \triangleq \mathbf{g}_{m,s\notin S^{\text{overflow}}}$. Hence, it consists only of those elements s in $\mathbf{g}_m$ whose indices are *not* in S^{overflow}. It can be shown that

$$\mathbf{g}_m^{\text{eff}} \parallel \mathbf{1}_{1,N-|S^{\text{overflow}}|} \tag{26}$$

is a necessary condition for stagnation of row m.

An algorithm is intended to detect a local minimum of the core, and then escape it:

1. Execute the *minimization core* given in App. A once. Use its output multiplexing code and corresponding MSE to initialize $\mathbf{W}^0$ and $\widetilde{\text{MSE}}^{\text{min}}$
2. Iterate the subsequent steps 3,4,5 until an upper limit on the number of iterations is met. The iteration index is l.
3. For all $m \in \{1,\ldots,N\}$ if Eq. (26) holds, then row m is detected as stagnated. Replace it by a random row vector. This new row complies with (17, 23) and is formulated as described in App. B.
4. Execute the *minimization core* again. Use the modified $\mathbf{W}^{(l-1)}$ as its initial solution. Its output is $\mathbf{W}^{(l)}$, as well as $\widetilde{\text{MSE}}^{(l)}$ and its corresponding gradient $\mathbf{\Gamma}^(l)$.
5. If $\widetilde{\text{MSE}}^{(l)} < \widetilde{\text{MSE}}^{\text{min}}$ Then $\widetilde{\text{MSE}}^{\text{min}} := \widetilde{\text{MSE}}^{(l)}$.

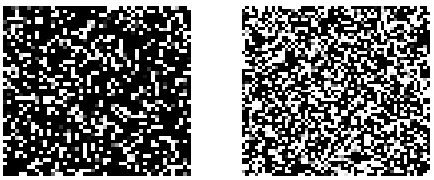

Figure 5. Multiplexing codes produced by our algorithm. [Left] $N = 47, C = 12$. [Right] $N = 57, C = 24$. Here, black pixels denotes $w_{m,s} = 0$. White denotes $w_{m,s} = 1$. The intermediate values are in gray.

6. Multiplexing Methodology

This section outlines our methodology of multiplexing light sources, considering photon noise and saturation. As a first step, estimate the noise parameters κ_{gray}^2 and η^2 of the acquisition system. These parameters directly yield χ^2. The second step is to calculate optimal multiplexing codes, ignoring photon noise, per $C \leqslant \frac{N+1}{2}$. This can be done by the algorithm described in Sec. 5. As an examples, Fig. 5 shows multiplexing codes produced by our numerical procedure for two pairs of N and C values. The multiplexing codes and the noise parameters of the camera are used by the algorithm is Sec. 4 to find the optimal value of C. Then, the desired multiplexing code $\mathbf{W}$ is the one corresponding to this value of C. As an example, Fig. 6 plots the multiplex gain corresponding to some noise parameters and codes: the plot highlights the curve corresponding to the noise characteristics encountered in our experiments. Notice the shift in

[3] A valid inverse of a matrix A can never be nulled. If it could, it would have yielded a contradiction: $\mathbf{A}^{-1}\mathbf{A} = \mathbf{I}_{N\times N} = \mathbf{0}_{N\times N}\mathbf{A}$, where $\mathbf{0}_{N\times N}$ is an $N \times N$ null matrix.

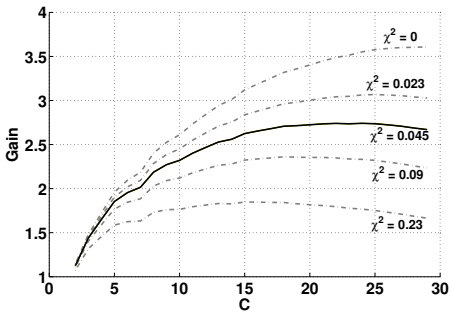

Figure 6. The expected multiplex gain for various C and χ^2 values. Here $N = 57$, thus $C \in \{2, \ldots, 29\}$. The solid line corresponds to our system's χ^2. The C that maximizes $G(C)$ shifts as the relative signal-dependency of the noise varies.

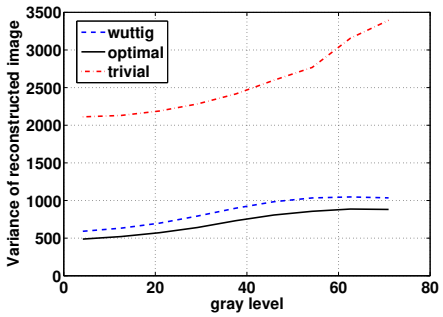

Figure 7. MSEs obtained by decoding process of illumination multiplexed images ($N = 57$). Our optimal code outperforms both Wuttig's [38] code and trivial illumination.

the location of the gain's peak, as the signal dependency of the noise increases. This stems from the fact that photon noise inhibits the use of more light sources. On the other hand, if noise is totally signal-independent, it is best to use the maximal number of sources, as in the **S**-matrix.

7. Experiments

We now demonstrate multiplexing with the codes obtained by our algorithm. We apply these codes to multiplex light sources considering photon noise and saturation effects on the acquired images. The experiment setting included a PGR dragonfly camera controlled by a computer, mounted with a 35mm Nikon lens. Illumination sources were created by an EPSON EMP-7800 projector that projected patterns of light rectangles onto a white wall (see ref. [32]). All frames were taken with an exposure time of 63 milliseconds. This exposure time meets the frequency limitation of 15Hz. It also eliminates illumination source intensity fluctuations measured to occur in cycles of 7 milliseconds.

As explained in Sec. 6, we preformed a calibration session. It was based on 10 frames sequences for each number of activated light sources. We estimated the gray-level variance at each pixel. As a representative value for each number of the light sources we averaged the estimated variance over the entire image. This statistics generally agreed with the affine noise model. The estimated values of the noise parameters for $N = 57$ are $\kappa_{\text{gray}} = 42.4$[gray levels]; $\eta = 9.0$ [gray levels/light sources]; $\chi^2 = 0.045$

Following the calibration session we created multiplex codes for our test case. For $N = 57$ we used the Identity matrix $\mathbf{I}_{57}$, a matrix offered by Wuttig [38] and a matrix produced by our algorithm. The multiplex code offered by Wuttig uses eight fully activated light sources for each measurement. Note that the optimal number of fully activated sources has been evaluated, using the derivations in [38], to be 20. However, this value does not correspond to a valid matrix. Our algorithm, described in sec. 4 determined a budget of 24 fully operated light sources for each measurement.

Once the multiplex codes had been constructed, we utilized them to illuminated a scene while acquiring image sets. From each set of acquired images, we reconstructed the scene as if illuminated by individual illumination sources. Fig. 1 for an example of a demultiplexed image. For each image set, we estimated the noise statistics. The results of the MSE evaluation are shown in Fig. 7. As predicted by the analytical derivations, the best multiplex sequence for the signal dependent noise (as modelled here) is the sequence created by our method.

The following scenario examines the effects of saturation due to specular areas in the acquired frame. In a similar manner to the case of $N = 57$ we calibrated the noise parameters of the camera and scene. The noise parameters for this case are $\kappa_{\text{gray}} = 74.0$[gray levels]; $\eta = 28.7$ [gray levels/light sources]; $\chi^2 = 0.15$.

We then constructed multiplex codes for the case of $N = 47$ and $N = 11$. We examined multiplex codes based on **I**, **S**-matrices and the matrices produced by our numerical algorithm. The latter uses the equivalence of 12 light sources, tuned for maximal intensity, for $N = 47$ and 5 sources for $N = 11$.

The resulting reconstruction of images with individual source illumination for $N = 47$ are shown in Fig. 8 and the MSE estimation for both cases is shown in Fig. 9.

While acquiring the images using $N = 47$ and the **S**-matrix based multiplex code, the specular parts of the images have been saturated. Although most of the image is dark (with gray levels of up to 1000), the specularities caused us to exploit all of the dynamic range. The saturation rules out the possibility of using Hadamard codes, for this case altogether. We have shown the statistics of the vast majority of the pixels in the image that are not saturated in an intention to prove the dual advantage of our method. We

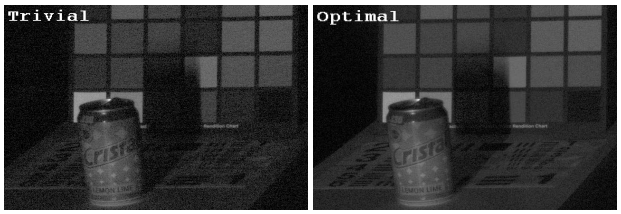

Figure 8. [Left] An image taken under a single light source. [Right] An image of the same scene, decoded from multiplexed illuminated objects. It is decoded as if illuminated by the same single source. The multiplexing code is optimal.

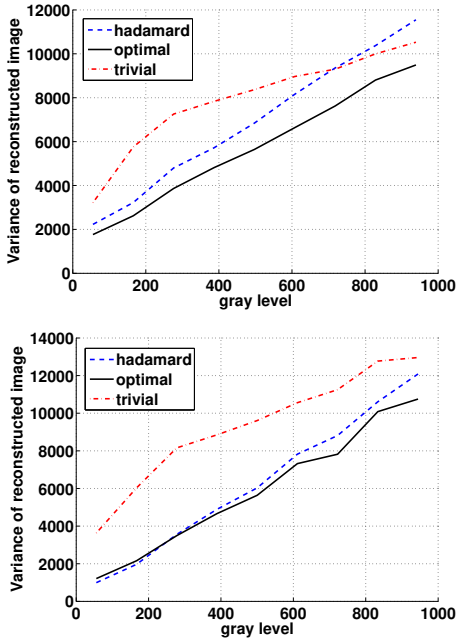

Figure 9. The MSEs of decoded images derived from illumination multiplexed frames. [Top] Hadamard multiplexing becomes counter productive for high gray levels while our multiplexing code is better than the trivial one (and the Hadamard code) all along the dynamic range . [Buttom] 47 light sources. Some pixels became saturated when multiplexed by a Hadamard code. This invalidated the use of Hadamard code.

are able to construct multiplex codes that surpass the trivial codes, in cases where other codes simply do not exist. Even when other codes do exist, the codes based on our method are better adapted to the scenario, hence producing smaller MSE of the reconstructed images.

8. Discussion

Our approach provides optimal multiplexing codes for every desired number of light sources N and radiance inhibition (saturation, photon noise). It does so for much more general cases than those reported in the literature, covering cases for which no codes are known. By accounting for fundamental physical limits in image acquisition, it achieves results that are superior to other multiplexing codes, when such competing codes exist. Future research may improve the methods used for optimization. Our work may apply to many applications that use multiplexing in general, beyond multiplexing of illumination sources (Xray, spectroscopy etc.).

A. Minimization Core

We iterate on k, minimizing $\widetilde{\text{MSE}}$ as a function of $\mathbf{W}$. The algorithm stops when $|\widetilde{\text{MSE}}_k - \widetilde{\text{MSE}}_{k+1}| < \epsilon$, where ϵ is a pre-determined small threshold.

1. For given N and C create an initial matrix $\mathbf{W}_0$ (See App. B). The initial matrix $\mathbf{W}_0$ complies with constraints (21,22,23).
2. Repeat the subsequent stages 3 and 4, until the improvement in $\widetilde{\text{MSE}}$ is negligible.
3. Calculate the gradient in $\mathbf{W}_k$ as appears in Eq. (25). Then, calculate an updated matrix $\mathbf{W}_{k+1}^{\text{unconst}} \triangleq \mathbf{W}_k - \mathbf{\Gamma}_k$, as in standard gradient descent. We take care of the step size in stage 4.
4. Project $\mathbf{W}_{k+1}^{\text{unconst}}$ in the following way:
   (i) Project $\mathbf{W}_{k+1}^{\text{unconst}}$ onto the hyperplane used in (23). It is easy to show that for each row, $\mathbf{w}_m^{\text{unconst}}$, its projection is
   $$\mathbf{w}_m^{\text{proj}} = \mathbf{w}_m^{\text{unconst}} + \left[C - \sum_{s=1}^{N} w_{m,s}^{\text{unconst}} \right] \frac{\mathbf{1}_{1,N}^t}{N} \quad . \tag{27}$$
   (ii) Denote $\mathbf{d}_k \triangleq \mathbf{W}_{k+1}^{\text{proj}} - \mathbf{W}_k$. Update $\mathbf{W}_{k+1}^{\text{unbounded}} = \mathbf{W}_k - \beta \mathbf{d}_k$, where β is a parameter controlling the step size.
   (iii) Project $\mathbf{W}_{k+1}^{\text{unbounded}}$ onto constraints (21,22) to create $\mathbf{W}_{k+1}$. This is done by truncating the elements of $\mathbf{W}_{k+1}^{\text{unbounded}}$'s values to $[0, 1]$.

B. Initialization of the Minimization Core

We now describe the initialization procedure for the initial solution $\mathbf{W}_0$. We randomly generate values between 0.1 and 0.9. This is done to avoid dictation of the active constraints by the initial solution. We then normalize the rows of $\mathbf{W}_0$ to have the sum of C. Any element violating (17) is regenerated and the normalization process is repeated until full satisfaction of (17, 23).

References

[1] F. Alter, Y. Matsushita, and X. Tang. An intensity similarity measure in low-light conditions. In *Proc. ECCV Vol. 4*, pages 267–280, 2006. 2

[2] H. H. Barrett and W. Swindell. *Radiological Imaging*, volume 1. Academic, New York, 1981. 2

[3] R. Basri and D. Jacobs. Lambertian reflectance and linear subspaces. *IEEE Trans. PAMI*, 25:218–233, 2003. 1

[4] D. P. Bertsekas. *Nonlinear Programming*. Athena Scientific, 1999. 4, 5

[5] O. G. Cula, K. J. Dana, D. K. Pai, and D. Wang. Polarization multiplexing for bidirectional imaging. In *Proc. CVPR Vol. 2*, pages 1116–1123, 2005. 1

[6] P. Debevec. Image-based lighting. *IEEE Computer Graphics and Applications*, 22:26–34, 2002. 1

[7] H. Farid and E. H. Adelson. Separating reflections and lighting using independent components analysis. In *Proc. CVPR Vol. 1*, pages 262–267, 1999. 1

[8] T. J. Fellers and M. W. Davidson. CCD noise sources and signal-to-noise ratio, 2004. in Optical Microscopy Primer Molecular Expressions$^{\mathrm{TM}}$, Florida State U.S. 2

[9] E. E. Fenimore and T. M. Cannon. Coded aparture imaging with uniformly redundent arrays. *Applied Optics*, 17:337–347, 1978. 2

[10] D. Goldman, B. Curless, A. Hertzmann, and S. M. Seitz. Shape and spatially-varying BRDFs from photometric stereo. In *Proc. ICCV*, pages 341–348, 2005. 1

[11] M. Harwit and N. J. A. Sloane. *Hadamard Transform Optics*. Academic, New York, 1979. 2, 3, 4

[12] M. Hatzitheodorou. Shape from shadows, a hilbert space setting. *J. Complex.*, 14:63–84, 1998. 1

[13] G. Healey and T. O. Binford. Local shape from specularity. In *Proc. ICCV*, pages 151–160, 1987. 1

[14] B. P. K. Horn. *Robot Vision*. MIT, 1986. 1

[15] S. Ioué and K. R. Spring. *Video Microscopy*, 2^{nd} ed., 1997. ch. 6,7,8, Plenum Press, New York. 2

[16] K. C. Lee, J. Ho, and D. J. Kriegman. Acquiring linear subspaces for face recognition under variable lighting. *IEEE Trans. PAMI*, 27:684–698, 2005. 1

[17] H. Lensch, J. Kautz, M. Gosele, W. Heidrich, and H. Seidel. Image-based reconstruction of spatial appearance and geometric detail. *ACM TOG*, 22:234–257, 2003. 1

[18] M. Levoy, B. Chen, V. Vaish, M. Horowitz, I. McDowall, and M. Bolas. Synthetic aperture confocal imaging. *ACM TOG*, 23:825–834, 2004. 1

[19] C. Liu, W. T. Freeman, R. Szeliski, and S. B. Kang. Noise estimation from a single image. In *Proc. CVPR Vol. 1*, pages 901–908, 2006. 2

[20] Q. T. Luong, P. Fua, and Y. Leclerc. Recovery of reflectances and varying illuminants from multiple views. In *Proc. ECCV Vol. 3*, pages 163–179, 2002. 1

[21] T. Malzbender, D. Gelb, and H. Wolters. Polynomial texture maps. In *Proc. ACM SIGGRAPH*, pages 519–528, 2001. 1

[22] S. R. Marschner, S. H. Westin, E. P. F. Lafortune, and K. E. Torrance. Image-based bidirectional reflectance distribution function measurement. *Applied Optics*, 39:2592–2600, 2000. 1

[23] W. Matusik, H. Pfister, A. Ngan, P. Beardsley, R. Ziegler, and L. McMillan. Image-based 3D photography using opacity hulls. *ACM TOG*, 21:427–437, 2002. 1

[24] F. Moreno-Noguer, S. K.Nayar, and P. N. Belhumeur. Optimal illumination for image and video relighting. In *Proc. CVMP*, pages 201–210, 2005. 1

[25] Y. Moses, S. Ullman, and S. Edelman. Generalization to novel images in upright and inverted faces. *Perception*, 25:443–461, 1996. 1

[26] G. Nitzsche and R. Riesenberg. Noise, fluctuation and HADAMARD-transform-spectrometry. In *Proc. SPIE*, volume 5111, pages 273–282, 2003. 2

[27] M. Osadchy and D. Keren. Efficient detection under varying illumination conditions and image plane rotations. *Computer Vision & Image Understanding*, 93:245–259, 2004. 1

[28] J. A. Paterson, D. Claus, and A. W. Fitzgibbon. BRDF and geometry capture from extended inhomogeneous samples using flash photography. In *Proc. EUROGRAPHICS*, 2005. 1

[29] R. Ramamoorthi and P. Hanrahan. Frequency space environment map rendering. *ACM TOG*, 21:517–526, 2002. 1

[30] R. Raskar, K. H. Tan, R. Feris, J. Yu, and M. Turk. Nonphotorealistic camera: depth edge detection and stylized rendering using multiflash imaging. *ACM TOG*, 23:679–688, 2004. 1

[31] I. Sato, T. Okabe, Y. Sato, and K. Ikeuchi. Using extended light sources for modeling object apperance under varying illumination. *Proc. ICCV*, pages 325–332, 2005. 1

[32] Y. Y. Schechner, S. K. Nayar, and P. N. Belhumeur. A theory of multiplexed illumination. In *Proc. ICCV Vol. 2*, pages 808–815, 2003. 1, 2, 3, 6

[33] P. Sen, B. Chen, G. Garg, S. R. Marschner, M. Horowitz, M. Levoy, and H. P. A. Lensch. Dual photography. *ACM TOG*, 24:745–755, 2005. 1

[34] A. Shashua. On photometric issues in 3D visual recognition from a single 2D image. *IJCV*, 21:99–122, 1997. 1

[35] T. Sim, S. Baker, and M. Bsat. The CMU pose, illumination and expression database. *IEEE Trans. PAMI*, 25:1615–1618, 2003. 1

[36] G. K. Skiner. X-ray imaging with coded masks. *Scientific American*, 259:84–89, 1988. 2

[37] A. Wenger, A. Gardner, C. Tchou, J. Unger, T. Hawkins, and P. Debevec. Performance relighting and reflectance transformation with time-multiplexed illumination. *ACM TOG*, 24:756–764, 2005. 1, 2, 3

[38] A. Wuttig. Optimal transformations for optical multiplex measurements in the presence of photon noise. *Applied Optics*, 44:2710–2719, 2005. 3, 6

[39] A. Yuille, J. M. Coughlan, and S. Konishi. The KGBR viewpoint-lighting ambiguity. *JOSA A*, 20:24–31, 2003. 1

[40] T. Zickler. Reciprocal image features for uncalibrated helmholtz stereopsis. In *Proc. CVPR Vol. 2*, pages 1801–1808, 2006. 1